(Received 17 September 2025, Accepted 11 November 2025, Scheduled 16 December 2025)

Dielectric Response and Transient Potential Characteristics of Grounding Electrodes Considering the Frequency Effect of Frozen Soil

Wei Shen[1,*], Mingxi Zhu[1], Xinmin Li[1], and Ziming He[2]

[1] *Electric Power Research Institute of State Grid, Shaanxi Electric Power Company Limited, Xi'an 710654, China*
[2] *China Electric Power Research Institute, Beijing, China*

ABSTRACT: This study investigates the electrical characteristics of grounding electrodes in seasonal frozen soil through experimental and simulation approaches. Experimental measurements reveal the variation patterns of soil resistivity and dielectric constant within the frequency range of 100 Hz–10 MHz at different temperatures. The results indicate that decreasing temperature leads to increased resistivity and decreased dielectric constant, with both parameters tending to stabilize at high frequencies. Computations based on the method of moments demonstrate that accounting for the frequency dependence of frozen soil reduces the impedance magnitude by 20%–40% in the high-frequency range and results in more complex resonant behavior. When the length of the grounding electrode is less than the freezing depth, the high-frequency capacitive effect is significantly enhanced. Time-domain analysis shows that under lightning impulse conditions, the potential reduction is approximately 22% during the first return stroke and can reach up to 42% in subsequent return strokes. The study concludes that the frequency dependence of the electrical parameters of frozen soil has a considerable influence on the response of grounding electrodes and should be considered in modeling and lightning protection design.

1. INTRODUCTION

Lightning activity is frequent in the western plateau regions of China, where seasonal frozen soil is widely distributed. The phase change of water in frozen soil induces fundamental differences in its electrical properties relative to unfrozen soil [1–3], significantly affecting the lightning protection performance of power system grounding devices [4, 5]. However, existing research is mainly concentrated on unfrozen soil at normal temperatures [6], and there is a lack of systematic experimental data on the resistivity and dielectric constant of frozen soil within the lightning current frequency range (kHz–MHz) [7], which will result in deviations in lightning transient analysis. Although related studies in remote sensing have been conducted, they mainly concentrate on microwave frequencies and are not directly applicable to lightning protection issues in power systems [8–10].

Integrating experiment and simulation, this paper investigates the electrical behaviour of grounding electrodes in seasonally frozen soil. Resistivity and permittivity of soil samples were first measured from 100 Hz to 10 MHz under varying temperature and moisture; their pronounced frequency dependence [11] was quantified. Wide-band impedance of electrodes under different frozen-layer thicknesses and burial depths was then analysed via the method of moments. Time-domain simulations further examined transient-potential responses under lightning impulse [12, 13], providing theoretical guidance for the lightning protection design of transmission lines in permafrost regions.

2. EXPERIMENTAL PRINCIPLE AND METHODOLOGY

The main test equipment included an impedance analyzer (Keysight E5061B), a four-electrode probe, a temperature-controlled chamber (operating range: $-30°C$ to $+30°C$), precision temperature sensors, as well as devices for moisture content adjustment and dry density control. The test soil (loess from Shaanxi) samples were first sieved through a 2 mm mesh, and the initial moisture content was adjusted to 12%. The samples were then sealed 48 hours to homogenize. Then, the soil was compacted in 3 equal layers into a cylindrical test cell ($\Phi 150 \times 200$ mm) to ensure a uniform dry density. After assembly, the sample was placed in a temperature-controlled chamber, with preset test temperatures of $+20°C$, $0°C$, $-10°C$, and $-20°C$. At each temperature point, measurements commenced only after the temperature at the center of the sample stabilized within a difference of less than $0.3°C$ from the target value and was maintained for at least 30 minutes. All test cables were 50 Ω coaxial types, with single-point grounding and shielding measures implemented to minimize parasitic interference.

With copper electrodes ($\Phi 140$ mm) on opposite sides of the test box, the sandbox can be represented as a single-port circuit network whose equivalent circuit consists of a parallel combination of capacitance and conductance in Figure 1 [14], evalu-

* Corresponding author: Wei Shen (47598910@qq.com).

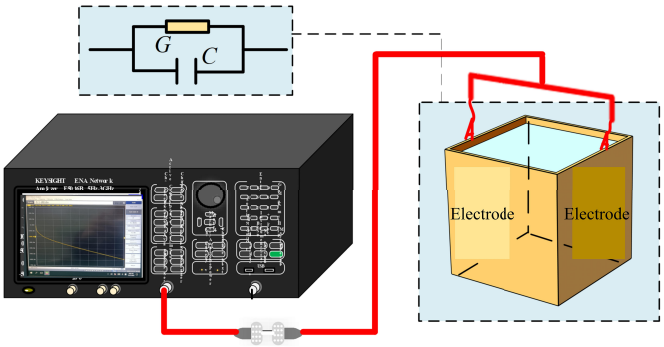

FIGURE 1. Soil sample swept-frequency parameter test platform.

ated via Equations (1)–(2).

$$Y = G + j\omega C \tag{1}$$

$$Y = \frac{A}{d}(\sigma^* + j\omega\varepsilon^*) \tag{2}$$

where G is the conductance (S); ω is the angular frequency (rad/s); C is the capacitance (F); A is the electrode surface area (m^2); d is the distance between the electrodes (m); σ^* is the complex conductivity in the frequency domain (S/m); and ε^* is the complex permittivity (F/m). Under sinusoidal excitation, the soil conductivity and dielectric constant can be expressed by Equation (3) [14].

$$\begin{cases} \sigma^* = \sigma' + j\sigma'' \\ \varepsilon^* = \varepsilon' - j\omega\varepsilon'' \end{cases} \tag{3}$$

Substituting Equation (3) into Equation (2) yields an alternative expression for the admittance Y, as shown in (4).

$$Y = \frac{A}{d}(\sigma_{eff} + \mathrm{j}\omega\varepsilon_0\varepsilon_{reff}) \tag{4}$$

This study employed scattering parameter method based on an impedance network analyzer to measure S-parameters of a single-port circuit network. Prior to measurement, the network analyzer was calibrated using open-circuit, short-circuit, and load calibration procedures. The calibrated analyzer was then connected to both ends of the soil sample via fixtures. After obtaining the S-parameters, the admittance parameters (Y-parameters) of the port were derived using Equation (5) [15] and (6), which can then be converted to obtain the resistivity and relative permittivity of the frozen soil at different frequencies.

$$Y = \frac{(1-S)}{Z_0(1+S)} \tag{5}$$

$$\begin{cases} \rho_{eff}(f) = \frac{1}{\sigma_{eff}} = \frac{A}{\mathrm{Re}(Y)\cdot d} \\ \varepsilon_{reff}(f) = \frac{\mathrm{Im}(Y)\cdot d}{\omega\varepsilon_0\cdot A} \end{cases} \tag{6}$$

where Z_0 is the matching impedance of 50 Ω, and ε_0 is the vacuum permittivity with a value of 8.854×10^{-12} F/m.

3. RESULTS AND ANALYSIS

The variations in relative permittivity and resistivity with frequency were measured for soil with an initial water content of 12% at temperatures of 13°C, −5°C, and −12°C, respectively. The measurement results are shown in Figures 2 and 3. The horizontal coordinate represents the common lightning current frequency range, spanning from 100 Hz to 10 MHz.

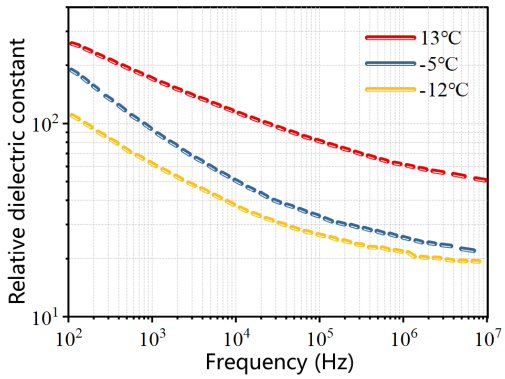

FIGURE 2. Frequency characteristics of soil relative permittivity at different temperatures.

As shown in Figure 2, the relative permittivity of the soil is the higher at positive temperatures than negative temperatures. This is because negative temperatures cause water in the soil to freeze into ice, and the permittivity of ice is much lower than that of water. When the soil temperatures are −5°C and −12°C, respectively, the difference in permittivity across frequencies is relatively small compared to that at positive temperatures. This phenomenon occurs because the water content in the soil decreases exponentially with decreasing temperature at subzero conditions: it declines rapidly near the phase transition temperature (around 0°C) and then gradually approaches zero as the temperature further decreases. Consequently, the water content — and thus the relative permittivity — differs only marginally between −5°C and −12°C. In the lightning current frequency range, the dominant contribution to the variation in the dielectric constant of moist soil is the orientational polarization of water molecules. As the excitation frequency increases, the rotational speed of dipoles gradually fails to keep pace with the changes in the electric field, leading to a gradual decrease in the relative permittivity of the soil. Consequently, the curves in Figure 2 tend to flatten out in the high-frequency range.

Figure 3 illustrates the variation of soil resistivity with frequency. As shown in the figure, soil resistivity increases with decreasing temperature, with particularly pronounced changes observed on both sides of the phase transition temperature. Experimental measurements indicate that the electrical parameters of frozen soil exhibit significant temperature and frequency dependence. When the temperature decreased from 13°C to −12°C, the soil resistivity increased sharply from 100 Ω · m to 4200 Ω · m (measured at 100 Hz), while the relative permittivity decreased markedly due to the freezing of water into ice (from approximately $\varepsilon \approx 80$ for liquid water to $\varepsilon\infty = 8$ for ice). Frequency-domain analysis reveals that within the lightning current frequency range of 100 Hz to 10 MHz, the permit-

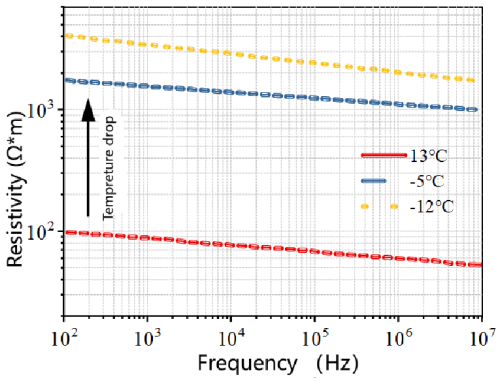

FIGURE 3. Frequency characteristics of soil resistivity at different temperatures.

tivity of frozen soil decreases with increasing frequency and stabilizes in the high-frequency range ($> 1\,\text{MHz}$). Resistivity also demonstrates frequency dependence, though this effect is negligible in thawed soil ($\rho < 100\,\Omega \cdot \text{m}$). These findings provide critical parameters for the modeling of grounding devices.

4. CALCULATION OF FREQUENCY-DOMAIN CHARACTERISTICS OF GROUNDING DEVICES IN SEASONAL FROZEN SOIL

4.1. Calculation Principles and Models

This study employs the Method of Moments (MoM), an electromagnetic computational technique, to solve the full-wave frequency-domain electromagnetic field equations. When the nonlinear characteristics of soil resistivity under lightning current are not considered, the MoM offers significant advantages: it eliminates the need for discretizing the entire soil dispersion region, requires no definition of absorbing boundary conditions [16], and only necessitates segmental discretization of the grounding electrode itself. Compared to Finite-Difference Time-Domain (FDTD) method and Finite Element Method (FEM), MoM achieves faster computational speeds and lower memory consumption, enabling efficient solutions for a large number of discrete frequency points within a single program execution. The frequency-domain full-wave electromagnetic field equations based on Maxwell's theory are expressed as follows (7).

$$\begin{cases} \theta = \sigma + \mathrm{j}\omega\varepsilon \\ \gamma^2 = \mathrm{j}\omega\mu\theta \\ \mathbf{A} = \frac{\mu I}{4\pi}\int \frac{e^{-\gamma R}}{R}\mathbf{ds} \\ U = -\frac{1}{\mu\theta}\nabla\cdot\mathbf{A} \end{cases} \tag{7}$$

where σ is the medium conductivity (S/m), ε the permittivity (F/m), ω the angular frequency of excitation (rad/s), μ the permeability (H/m), A the vector magnetic potential (Wb/m), R the distance from the observation point to the source (m), I the unit input current (A), d^*s^* the differential segment of the source (m), and U the transient potential response at the input point (relative to infinity) (V). The full-wave electromagnetic field equations incorporate both the induced electric field ($E = -\mathrm{j}\omega A - \nabla\varphi$) and displacement current density term ($\mathrm{j}\omega\varepsilon E$), thereby accounting for the inductive effects of the grounding device and capacitive effects of the soil. The impedance of the grounding electrode in the frequency domain can be expressed as (8).

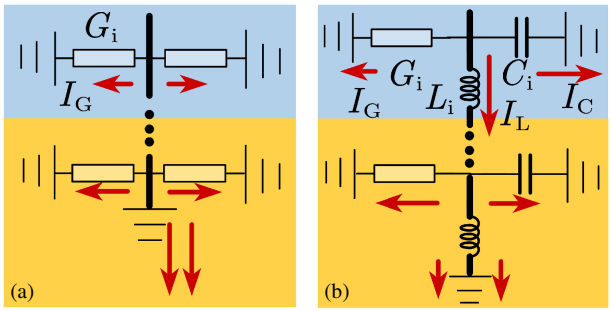

FIGURE 4. Equivalent circuit models of grounding electrodes across different frequency ranges: (a) Low-frequency leakage current distribution; (b) High-frequency leakage current distribution.

$$Z(\mathrm{j}\omega) = \frac{U(\mathrm{j}\omega)}{I(\mathrm{j}\omega)} \tag{8}$$

Electrical parameters of the surface layer of seasonal frozen soil are not fixed but vary significantly with climatic and temporal factors due to cyclic freezing and thawing in response to external temperature changes. Based on the experimental results presented in Section 3, the surface soil layer in this section is modeled as frozen soil at $-12°\text{C}$, while the underlying thawed soil, which is less affected by external environmental variations, is set as thawed soil at $13°\text{C}$.

The concept of "critical frequency" (F_{ci}) is introduced here [17]. When grounding systems are analsyzed, a key parameter is grounding resistance [18]. However, the value of grounding resistance is not constant and is strongly dependent on the frequency of the current. Above and below the critical frequency, the grounding impedance transitions from purely resistive to either inductive or capacitive in nature, as shown in Figure 4.

When $f < F_c$, the magnitudes of ωL for the grounding electrode and ωC for the soil are both small, so the phase angle is approximately zero. In this work, a grounding impedance is regarded as purely resistive when the phase angle lies within $\pm 1°$, and its value is numerically equal to the direct-current grounding resistance, which can be obtained from the wave-tail steady-state of the lightning impulse transient [19]. Under such conditions, the equivalent circuit model of the grounding electrode is shown in Figure 4(a), comprising solely the soil conductance, with IG — the conduction current — dominating the dissipation pattern. For $f > F_c$, the grounding impedance deviates from the DC value; in the time domain, this deviation emerges during the wave-front transition of the lightning current. Therefore, numerical analyses can select the appropriate grounding electrode circuit model by evaluating F_c and the frequency spectrum of the lightning current to determine whether inductive and capacitive components must be included.

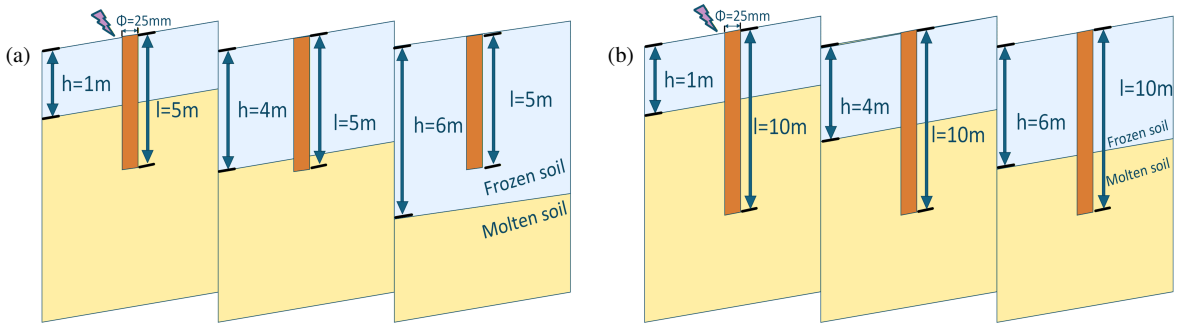

FIGURE 5. Schematic diagram of the layout of the calculation case. (a) The ground electrode length $l = 5\,\text{m}$. (b) The ground electrode length $l = 10\,\text{m}$.

4.2. Results and Analysis Incorporating the Frequency-Dependent Electrical Parameters of Seasonally Frozen Soil

When the frequency dependence of soil electrical parameters is ignored, the soil resistivity is fixed at the value corresponding to $f = 100\,\text{Hz}$, and the permittivity is set to the limit as frequency approaches infinity [20], denoted as ρ and $\varepsilon\infty$, respectively; the resulting soil parameters are listed in Table 1.

TABLE 1. Electrical parameters of soil with 12% initial water content.

Relative permittivity ($\varepsilon\infty$)	Resistivity ρ_0 ($\Omega \cdot$ m)
8($-12°$C)	4200($-12°$C)
8(13°C)	100(13°C)

As reported in reference, the frequency dependence of soil electrical parameters can be neglected when the resistivity is below $100\,\Omega \cdot \text{m}$ [21]. Therefore, the electrical parameters of thawed soil are treated as constant under the frequency components of lightning current, whereas the parameters of frozen soil, which are the focus of this study, must account for frequency dependence.

As illustrated in Figures 5(a) and (b), the vertical grounding electrode was modelled with a diameter of 25 mm and lengths $l = 5\,\text{m}$ and 10 m, while the surface frozen-soil thickness h was set to 1 m, 4 m, and 6 m.

Under 100 Hz–10 MHz excitation, this section conducts numerical evaluation via electromagnetic simulation on the frequency-domain response of vertical grounding electrodes of varying lengths in seasonally frozen soil and compares outcomes obtained with and without accounting for the frequency dependence of frozen-soil electrical parameters, as detailed in Figures 6–9.

In Figure 6, when $l < h$, the grounding electrode is entirely located within the frozen soil layer, as indicated by the legend "$h = 6\,\text{m}$" and the corresponding green vertical axis on the right. For frequencies above the critical frequency $f > F_c$, Figure 6 shows that the grounding impedance exhibits capacitive characteristics over a broad frequency range (approximately 2×10^4 to 4×10^6 Hz), with a negative phase angle. As the frequency increases, the capacitive behavior becomes more pronounced, and the magnitude of the impedance decreases more significantly. This phenomenon occurs because the high resistivity of frozen soil leads to a gradual increase in the ratio of displacement current J_c to conduction current J_G with increasing frequency, as described by Equation (9). Consequently, current dissipation becomes dominated by the displacement current I_c, resulting in a trend toward capacitive impedance.

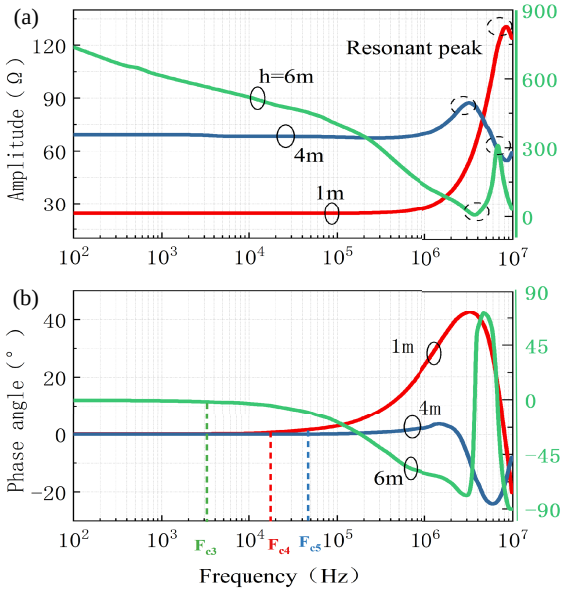

FIGURE 6. Amplitude-frequency and phase-frequency characteristics of grounding impedance for $l = 5\,\text{m}$ when considering frequency-independent electrical parameters of frozen soil.

$$\frac{J_c}{J_G} = \frac{\omega\varepsilon}{\sigma} = \rho\omega\varepsilon \tag{9}$$

However, when the frequency approaches approximately 5 MHz, the phase angle of the grounding impedance becomes positive, indicating a resonant peak. The impedance exhibits oscillatory characteristics, transitioning between inductive and capacitive behaviors across different frequencies. The equivalent circuit model under these conditions is shown in Figure 4(b), which consists of soil conductance G_i, capacitance C_i, and the inherent inductance L_i of the grounding device, connected in cascade.

In Figure 7, the length of the grounding electrode is $l = 10\,\text{m}$, meaning $h < l$. Under the three conditions of $h = 1$, 4, and 6 m, the critical frequency F_c is approximately equal, around

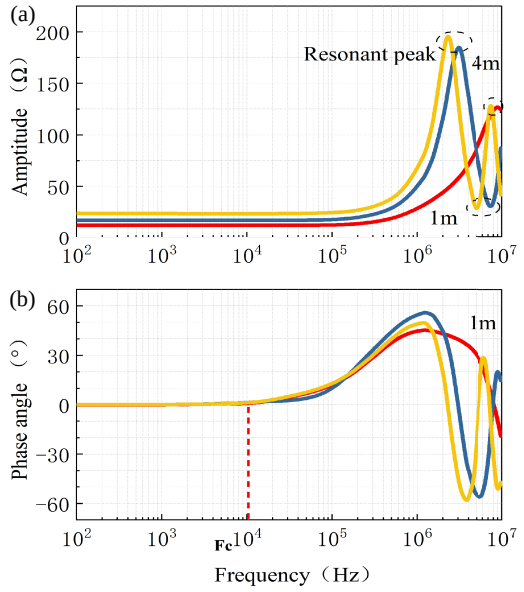

FIGURE 7. Amplitude-frequency and phase-frequency characteristics of grounding impedance for $l = 10$ m when considering frequency-independent electrical parameters of frozen soil.

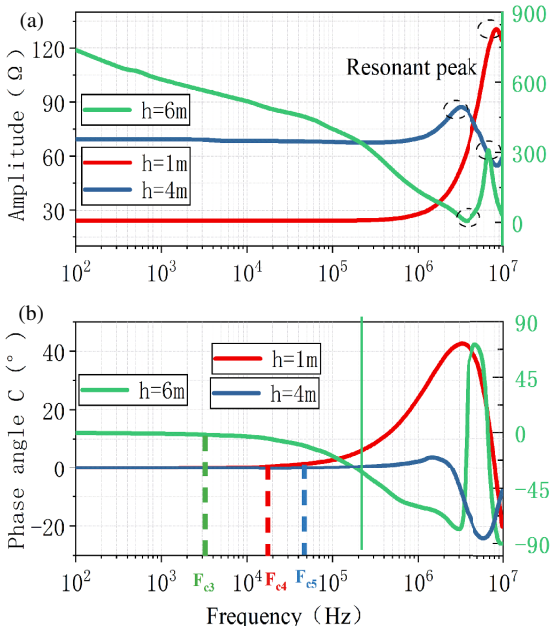

FIGURE 8. Ground impedance magnitude and phase characteristics versus frequency when $l = 5$ m, without considering frequency characteristics. (a) Frequency-dependent magnitude of the grounding impedance. (b) Frequency-dependent phase angle of the grounding impedance.

10 kHz. When $f > F_c$, for all three scenarios, both the phase angle and magnitude of the grounding impedance gradually increase with frequency and remain positive. This occurs because, at low frequencies, the primary current dissipation region of the grounding electrode is located in the low-resistivity thawed soil. As indicated by Equation (9), the capacitive effect of thawed soil is weak, and the inductive effect of the grounding electrode dominates.

For the cases where $h = 4$ m and 6 m, at higher frequencies, the inductive effect of the grounding electrode reduces current dissipation at its distal end, resulting in an effective length. Instead, current dissipation predominantly occurs in the surface frozen soil layer (as illustrated in Figure 6, where the length of the red arrows represents the relative magnitude of displacement and conduction leakage current densities). Under these conditions, the grounding impedance exhibits capacitive characteristics with a negative phase angle. Although $h < l$, the increased thickness of the surface frozen soil layer influences the high-frequency behavior of the grounding electrode. As shown by the black dashed line in Figure 7, a greater frozen soil thickness enhances the capacitive effect, shown as a lower frequency threshold for the onset of negative phase angles in the grounding impedance.

In this section, the electrical parameters of the frozen soil are not set as constant values but are defined as frequency-dependent. The data required for the calculations are sourced from Section 2.

When the frequency-dependent decrease in resistivity and permittivity of the surface frozen soil layer is considered, a comparison between Figure 6 and Figure 8, as well as Figure 7 and Figure 9, reveals the following: If $h > l$, the magnitude of the grounding impedance decreases significantly across the entire frequency range; if $h < l$, the decrease in impedance magnitude is primarily noticeable only in the high-frequency range.

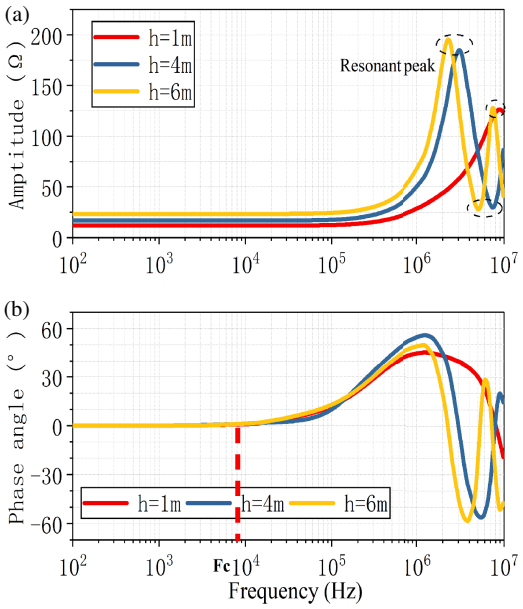

FIGURE 9. Ground impedance magnitude and phase characteristics versus frequency when $l = 10$ m, without considering frequency characteristics. (a) Frequency-dependent characteristic of grounding impedance magnitude. (b) Frequency-dependent characteristic of grounding impedance phase angle.

The high-frequency characteristics of the grounding impedance become more complex, exhibiting more pronounced oscillatory behavior and additional resonant peaks within the 1 MHz–10 MHz frequency band. Additionally, the critical frequency F_c of the grounding impedance becomes lower.

5. TRANSIENT POTENTIAL VARIATION OF GROUNDING ELECTRODES IN SEASONAL FROZEN SOIL

5.1. Calculation and Analysis of Transient Potential on Grounding Electrodes under First Return Stroke

The process of lightning current dissipation through the tower grounding device is an electromagnetic transient phenomenon on the microsecond (μs) timescale [21]. By employing the inverse Fourier transform, the frequency-domain solution can be converted into a transient solution in the time domain. Taking the transient potential response as an example (10):

$$V(t) = F^{-1}\left(Z(\mathrm{j}\omega) \cdot I(\mathrm{j}\omega)\right) \tag{10}$$

where $Z(\mathrm{j}\omega)$ is the frequency-domain grounding impedance, $I(\omega)$ the frequency-domain lightning current, and F^{-1} the inverse Fourier operator. Lightning strikes often involve multiple return strokes [22, 23]. In this study, Heidler function is used to model the lightning current source, as expressed in the following Equation (11):

$$I(t) = \frac{I_p}{\eta} \frac{(t/\tau_1)^n}{1 + (t/\tau_1)^n} e^{-t/\tau_2} \tag{11}$$

In the equation, I_p is the peak current (kA), τ_1 the front time (μs), τ_2 the tail time μs), n the integral exponent taken as 2, and η the correction factor. Lightning-current parameters are listed in Table 2; subsequent strokes are represented by the superposition of subsequent stroke 1 and subsequent stroke 2.

TABLE 2. Lightning-current parameters.

Lightning current	I_0	τ_1	τ_2	η
First stroke	28	1.8	95	0.8231
Subsequent stroke 1	10.7	0.25	2.5	0.6394
Subsequent stroke 2	6.5	2	230	0.8765

Figure 10 shows a typical lightning-current waveform. The amplitude of the subsequent stroke is approximately one-third that of the first stroke, but its front time is shorter, containing higher-frequency sinusoidal components.

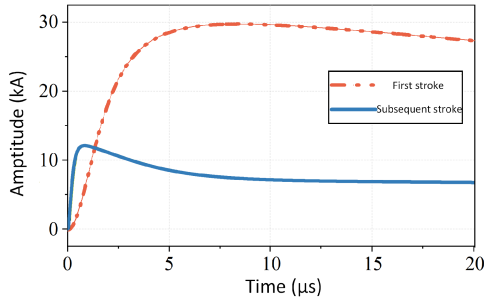

FIGURE 10. Typical first-stroke and subsequent-stroke current waveforms.

In Figure 11, the solid lines correspond to results obtained with frequency-independent frozen-soil parameters, whereas the scattered symbols incorporate full frequency dependence. Panel (a) shows the transient potential of a 10 m electrode: as the frozen-layer thickness h increases (but remains $h < l$), the peak potential rises, indicating that deeper surface freezing degrades the current-dissipation performance of the vertical electrode. When the frequency dependence of the frozen layer is included, the transient potential almost coincides with the frequency-independent case. This is because the dominant spectral content of the return stroke lies in the kHz band; at these low-frequency components most current dissipates in the thawed soil surrounding the electrode tip (Figure 11), so the frequency dependence of the surface frozen soil exerts only a marginal influence on the transient potential.

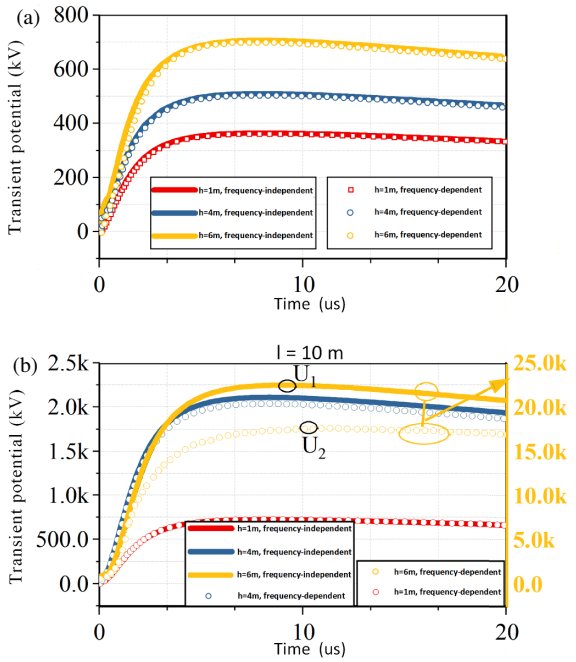

FIGURE 11. Transient potential of grounding electrodes with different lengths under first lightning stroke. (a) Transient potential under the first stroke when $l = 10$ m. (b) Transient potential under the first stroke when $l = 5$ m.

Figure 11 shows the transient-potential behaviour for a 5 m electrode (right-hand yellow axis corresponds to transient potential when $h = 6$ m, and the same applies to Figure 12). When $h = 6$ m, the frozen layer is thicker than the electrode ($h > l$), and the transient potential is an order of magnitude larger than for $h < l$. Accounting for the frequency dependence of the frozen-soil parameters markedly moderates the rising slope and reduces the peak amplitude; Equation (12) gives a potential-drop ratio D of 22%. This outcome is consistent with the $h = 6$ m traces in Figures 6(a) and 9(a): when frequency dependence is included, the grounding-impedance magnitude decreases with increasing frequency across the entire lightning-current spectrum.

$$D = \frac{U_1 - U_2}{U_1} = 22\% \tag{12}$$

U_1 and U_2 denote the peak transient potentials of the grounding electrode without and with the consideration of frequency-dependent characteristics of frozen soil, respectively.

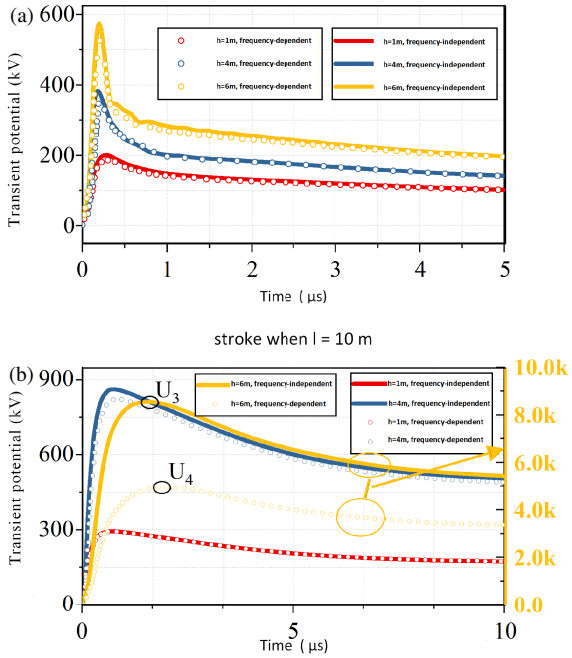

FIGURE 12. Transient potential of grounding electrodes with different lengths under subsequent lightning stroke. (a) Transient potential under the subsequent stroke when $l = 10\,\text{m}$. (b) Transient potential under the subsequent stroke when $l = 5\,\text{m}$.

5.2. Individual Fault-Type Diagnosis

Figure 12 shows the transient-potential behaviour of grounding electrodes of different lengths under subsequent strokes. Comparing the $h > l$ cases in Figure 11(b) and Figure 12(b) reveals that the transient-potential reduction is more pronounced for subsequent strokes when the frequency dependence of the surface frozen layer is considered; Equation (13) gives $D = 42\%$. This is because the grounding impedance becomes capacitive in the high-resistivity frozen soil, and the subsequent stroke contains higher-frequency sinusoidal components, causing the impedance magnitude to decrease more strongly under these high-frequency components.

$$D = \frac{U_3 - U_4}{U_3} = 42\% \tag{13}$$

U_3 and U_4 denote the peak transient potentials of the grounding electrode without and with the consideration of frequency-dependent characteristics of frozen soil, respectively.

6. CONCLUSION

By integrating experiment and simulation, this paper systematically investigates the electrical characteristics of grounding electrodes under seasonally frozen-soil conditions and further examines their lightning-induced transient-potential variations. The specific conclusions are as follows:

a) Accounting for the frequency dependence of frozen-soil electrical parameters reduces the grounding-impedance magnitude by roughly 20%–40% at high frequencies ($>$ 100 kHz) and introduces multiple resonance peaks between 1 MHz and 10 MHz, yielding a more complex resonant behaviour.

b) When electrode length exceeds the frozen-layer thickness, the low-frequency response is governed by the underlying thawed soil, and the characteristic frequency is $\approx 10\,\text{kHz}$; conversely, for $l < h$, the fully frozen surroundings intensify the high-frequency capacitive effect, expanding the negative-phase region by roughly 40%.

c) Increasing frozen-layer thickness markedly intensifies the frequency-dependence effect. At $h = 6\,\text{m}$, the high-frequency capacitive behaviour emerges roughly one decade earlier than at $h = 1\,\text{m}$, and the impedance-magnitude difference exceeds 30% in the high-frequency range.

d) Under lightning stroke, if the electrode is embedded in high-resistivity frozen soil, including the frequency dependence yields a potential drop of $\approx 22\%$ for the first return stroke and up to 42% for subsequent strokes, demonstrating that transient analyses of grounding electrodes in permafrost regions must incorporate the frequency-dependent effect.

ACKNOWLEDGEMENT

This work is supported by the research fund of State Grid Corporation of China (5500-202332532A-3-2-ZN).

REFERENCES

[1] Cai, W., C. Zhu, and W. Lein, "Temperature-and stress-dependent electrical responses of frozen soils," *Acta Geotechnica*, Vol. 20, 3835–3843, 2025.

[2] Tomaškovičová, S. and T. Ingeman-Nielsen, "Quantification of freeze-thaw hysteresis of unfrozen water content and electrical resistivity from time lapse measurements in the active layer and permafrost," *Permafrost and Periglacial Processes*, Vol. 35, No. 2, 79–97, 2024.

[3] Bai, L., J. Li, T. Liu, Z. Jiang, and D. Mao, "Seasonal frozen soil electrical resistivity estimation based on capillary fractal model," *Water Resources Research*, Vol. 61, No. 3, e2024WR038224, Mar. 2025.

[4] Salarieh, B., J. De Silva, and B. Kordi, "High frequency response of grounding electrodes: Effect of soil dielectric constant," *IET Generation, Transmission & Distribution*, Vol. 14, No. 15, 2915–2921, 2020.

[5] Akbari, M., K. Sheshyekani, and M. R. Alemi, "The effect of frequency dependence of soil electrical parameters on the lightning performance of grounding systems," *IEEE Transactions on Electromagnetic Compatibility*, Vol. 55, No. 4, 739–746, Aug. 2013.

[6] Sunjerga, A., M. Rubinstein, D. Poljak, M. Despalatović, G. Petrović, and F. Rachidi, "High-frequency response of a hemispherical grounding electrode," *Electric Power Systems Research*, Vol. 226, 109877, 2024.

[7] Wu, S., T. Zhao, J. Pan, H. Xue, L. Zhao, and J. Shi, "Improvement in modeling soil dielectric properties during freeze-thaw transitions," *IEEE Geoscience and Remote Sensing Letters*, Vol. 19, 1–5, 2022.

[8] Mialon, A., P. Richaume, D. Leroux, S. Bircher, A. A. Bitar, T. Pellarin, J.-P. Wigneron, and Y. H. Kerr, "Comparison of Dobson and Mironov dielectric models in the SMOS soil moisture retrieval algorithm," *IEEE Transactions on Geoscience and Remote Sensing*, Vol. 53, No. 6, 3084–3094, 2015.

[9] Zheng, D., X. Li, T. Zhao, J. Wen, R. Van Der Velde, M. Schwank, X. Wang, Z. Wang, and Z. Su, "Impact of soil per-

mittivity and temperature profile on L-band microwave emission of frozen soil," *IEEE Transactions on Geoscience and Remote Sensing*, Vol. 59, No. 5, 4080–4093, 2021.

[10] Visacro, S. and F. H. Silveira, "The impact of the frequency dependence of soil parameters on the lightning performance of transmission lines," *IEEE Transactions on Electromagnetic Compatibility*, Vol. 57, No. 3, 434–441, 2015.

[11] Kherif, O., S. Chiheb, M. Teguar, A. Mekhaldi, and N. Harid, "Time-domain modeling of grounding systems' impulse response incorporating nonlinear and frequency-dependent aspects," *IEEE Transactions on Electromagnetic Compatibility*, Vol. 60, No. 4, 907–916, 2018.

[12] Zhang, X., M. Shi, C. He, and J. Li, "On site oscillating lightning impulse test and insulation diagnose for power transformers," *IEEE Transactions on Power Delivery*, Vol. 35, No. 5, 2548–2550, 2020.

[13] Manjunath, A. D. B., F. Khan, N. Noyanbayev, N. Harid, H. Griffiths, R. P. Nogueira, N. T. C. De Oliveira, M. Haddad, and S. Ramanujam, "Investigation into variation of resistivity and permittivity of aqueous solutions and soils with frequency and current density," *IEEE Transactions on Electromagnetic Compatibility*, Vol. 64, No. 2, 443–455, 2022.

[14] Heidler, F., J. M. Cvetic, and B. V. Stanic, "Calculation of lightning current parameters," *IEEE Transactions on Power Delivery*, Vol. 14, No. 2, 399–404, 1999.

[15] Honarbakhsh, B., "Grounding system analysis: Microwave engineering approach," *IEEE Transactions on Electromagnetic Compatibility*, Vol. 63, No. 1, 74–81, 2021.

[16] Grcev, L., "Modeling of grounding electrodes under lightning currents," *IEEE Transactions on Electromagnetic Compatibility*, Vol. 51, No. 3, 559–571, 2009.

[17] Grcev, L., "Improved earthing system design practices for reduction of transient voltages," *Proc. CIGRE*, 1998.

[18] Cao, X., M. Wei, M. Wang, J. Liu, R. Li, and L. Yang, "Evaluation principle and method of horizontal grounding electrode based on time-varying impedance," *IET Science, Measurement & Technology*, Vol. 15, No. 2, 174–183, 2021.

[19] Sheshyekani, K. and M. Akbari, "Evaluation of lightning-induced voltages on multiconductor overhead lines located above a lossy dispersive ground," *IEEE Transactions on Power Delivery*, Vol. 29, No. 2, 683–690, 2014.

[20] Visacro, S. and R. Alipio, "Frequency dependence of soil parameters: Experimental results, predicting formula and influence on the lightning response of grounding electrodes," *IEEE Transactions on Power Delivery*, Vol. 27, No. 2, 927–935, 2012.

[21] Wang, S., Y. Gao, M. Chen, Z. Qiu, H. Zhuang, and R. Huang, "Instrumentation for sub-ampere lightning current measurement on a tall meteorological tower in complex electromagnetic environment," *Remote Sensing*, Vol. 16, No. 7, 1307, 2024.

[22] Shen, J., J. Gong, and D. Zhou, "Lightning return stroke positioning method based on CWT narrowband feature extraction," *Atmosphere*, Vol. 16, No. 3, 302, 2025.

[23] Shen, J., Z. Sun, L. Shi, and S. Qiu, "Analysis of time-domain characteristics of microsecond-scale repetitive pulse discharge events in lightning," *Atmosphere*, Vol. 16, No. 5, 606, 2025.